Global analysis of in situ cosmogenic ^{26}Al and ^{10}Be and inferred erosion rate ratios in modern fluvial sediments indicates widespread sediment storage and burial during transport

Christopher T. Halsted[1], Paul R. Bierman[2], Alexandru T. Codilean[3], Lee B. Corbett[2], Marc W. Caffee[4]

[1]Department of Geosciences, Williams College, Williamstown, MA 01267, USA
[2]Rubenstein School of Environment and Natural Resources, University of Vermont, Burlington, VT 05405, USA
[3]School of Earth, Atmospheric and Life Sciences and Australian Research Council Centre of Excellence for Australian Biodiversity and Heritage (CABAH), University of Wollongong, Wollongong NSW 2522, Australia
[4]Department of Physics and Astronomy, Purdue University, West Lafayette, IN 47907, USA

Correspondence to: Christopher T Halsted (ch22@williams.edu)

Abstract. Since the 1990s, analysis of cosmogenic nuclides, primarily ^{10}Be, in quartz-bearing river sand, has allowed for quantitative determination of landscape mass loss rates (hereafter, erosion rates) at a basin scale. Paired measurements of in situ cosmogenic ^{26}Al and ^{10}Be in sediment are less common but offer insight into the integrated exposure and burial history of sediment moving down slopes and through drainage basins. Prolonged burial (>10^5 years), a violation of assumptions underlying erosion rate calculations, is indicated by higher ^{26}Al-based than ^{10}Be-based erosion rates due to preferential loss of shorter-lived ^{26}Al by decay when quartz is at least in part shielded from cosmic rays.

Here, we use a global compilation of ^{26}Al and ^{10}Be data generated from quartz-bearing fluvial sediment samples (n = 766, including 117 new measurements) to calculate the discordance between erosion rates derived from each nuclide. We find that over 30% of samples (n = 234) exhibit discordance (> 2σ analytical uncertainty) between erosion rates derived from ^{10}Be and ^{26}Al, indicating sediment histories that include extended burial during residence on hillslopes and/or in the fluvial system after or during initial near-surface exposure. Physical basin parameters such as basin area, slope, and tectonic activity exhibit significant correlation with erosion rate discordance whereas climatic parameters have weak correlation, allowing us to infer the likelihood of sediment burial during transport in different geomorphic settings.

Paired ^{26}Al and ^{10}Be analyses in detrital fluvial samples provide a window into watershed processes, elucidating landscape behaviour at different spatial scales and allowing a deeper understanding of both sediment routing systems and whether methodological assumptions are violated. Although previous studies have found ^{26}Al/^{10}Be erosion rate discordance to be common in the world's largest drainage basins, our analysis suggests that such discordance also occurs regularly in basins as small as 1,000 km^2, indicating that sediment storage mechanisms are more complex than suggested by simple floodplain-area scaling laws. Moderately sized basins (1,000 – 10,000 km^2) with low average slopes in tectonically quiescent terrains appear conducive to extended sediment storage; thus, erosion rates from such basins are lower limits due to nuclide decay during storage. We find that sediment sourced from smaller, steeper basins in tectonically active regions is more likely to have similar ^{10}Be and ^{26}Al erosion rates indicative of limited storage and is thus more likely to provide reliable erosion rates.

1 Introduction

Fluvial sediments are a rich source of information about the upstream sediment routing system, which encompasses sediment generation, transport, and storage processes (Romans et al., 2016; Tofelde et al., 2021). For example, in situ cosmogenic ^{10}Be measurements of quartz isolated from fluvial sediments are used to estimate basin-averaged erosion rates. The application of this method in thousands of drainage basins around the world has provided valuable insights into physical and climatic controls on erosion (von Blanckenburg, 2005; Codilean et al., 2022; Portenga and Bierman, 2011; Schaefer et al., 2022). Such analyses assume an upstream sediment history in which material was generated through steady exhumation on hillslopes and then transported rapidly through fluvial networks, experiencing negligible storage while in transit (Bierman and Steig, 1996; von Blanckenburg, 2005; Granger et al., 1996; Granger and Schaller, 2014; Schaefer et al., 2022). Although erosion rates are now commonly measured, few studies have assessed the underlying assumptions of the technique and how often those assumptions are violated.

Sediment grains in fluvial systems can have a wide range of idiosyncratic transport and storage histories potentially spanning more than 10^6 years in large basins, as shown by cosmogenic nuclide analyses in modern fluvial sediments (Fülöp et al., 2020; Repasch et al., 2020; Wittmann et al., 2011), volumetric and geochemical analyses of valley fills (Blöthe and Korup, 2013; Jonell et al., 2018; Munack et al., 2016), and sediment transport models (Carretier et al., 2020). These complex sediment histories, along with the protracted sediment lag times, may confound reliable interpretation of upstream processes (Allen, 2008; Jerolmack and Paola, 2010). Sediment samples used for analysis of cosmogenic nuclides are typically amalgamations of thousands of grains, each of which has its own unique history.

Measuring multiple in situ cosmogenic radionuclides with different half-lives is a promising approach for discerning fluvial sediment histories (Codilean and Sadler, 2021; Schaefer et al., 2022). Calculating ratios between multiple cosmogenic radionuclides has provided insight into sediment provenance (e.g., Cazes et al., 2020) and storage histories (e.g., Wittmann et al., 2011; Fülöp et al., 2020; Ben-Israel et al., 2022) in river systems around the world. Such studies have helped test hypotheses about sediment dynamics in river basins, including that the integrated storage duration experienced by sediments on hillslopes and in floodplains is generally greater in larger basins (Wittmann et al., 2020), in post-orogenic regions (Cazes et al., 2020; Struck et al., 2018), and in arid regions (Makhubela et al., 2019). However, such hypotheses have yet to be tested on a global scale and questions remain, such as whether sediment storage duration scales with physical and/or climatological basin metrics.

In this study, we compiled measurements of paired in situ ^{26}Al and ^{10}Be concentrations in detrital fluvial sediment from around the world (n = 766, including 117 new ^{26}Al measurements on archived samples with previously published ^{10}Be measurements) to test for the existence and likelihood of fluvial sediment storage across a wide range of physical and climatological drainage basin settings. We account for localized differences in nuclide production ratios to facilitate comparison across the world and use a variety of statistical tests to assess relationships between isotope concentrations and basin-scale landscape and climate parameters. Such a global description provides insight into the complexity of river sediment transport and storage and allows us to evaluate the validity of

assumptions inherent to the widely-used, basin-scale cosmogenic nuclide erosion rate method (von Blanckenburg, 2005; Granger and Schaller, 2014; Schaefer et al., 2022).

2 Background

2.1 Sediment system dynamics and landscape change

Fluvial sediments are products of hillslope processes and are moved through sediment routing systems. These systems generally encompass regions of net sediment generation through bedrock weathering, regolith production, and sediment export from hillslope source zones (Allen, 2017). This detrital material is then transported by fluvial systems through riverine transfer zones and deposited in detrital sink zones (Schumm, 1977). Depending on the geometry of the riverine transfer zone, sediment storage may be transient (e.g., steep bedrock streams) or long lasting (e.g., lowland alluvial rivers). The extent and duration of storage in floodplains and sedimentary basins is an important control on weathering (e.g., Campbell et al., 2022; Dosseto et al., 2014) as well as on both the production of cosmogenic nuclides in sediments near the surface and the decay of those radionuclides if sediment is buried (Lal, 1991).

Understanding rates, controls, and dynamics of sediment generation and transport is important for quantifying landscape change over time and space (Allen, 2008; Romans et al., 2016). In many routing systems, river morphology (Langbein and Leopold, 1964; Leopold and Wolman, 1960) and floodplain volume (e.g., Otto et al., 2009) are determined by the sediment mass flux out of source zones, the rate of transit through transfer zones, and the accommodation space available for sediment storage. Changes to rates of sediment generation or transfer, primarily driven by tectonic or climatic forcings (Romans et al., 2016), can thus affect the behaviour of both sediment-supplying hillslopes and riverine transfer zones. Identifying such changes over space and through time is an important objective of geomorphological research and has prompted the development of tracer and rate-determining detrital geochronologic methods including measurements of cosmogenic nuclides, fission tracks, fallout radionuclides, and U/Th/He in various mineral phases (Allen, 2017).

2.2 Interpreting landscape processes from cosmogenic nuclides

The application of cosmogenic nuclide analyses to fluvial sediments, first using single nuclides (Bierman and Steig, 1996; Brown et al., 1995; Granger et al., 1996) and later paired nuclides (e.g., Clapp et al., 2000, 2001), has significantly advanced our understanding of geomorphology and sediment routing systems at a variety of spatial and temporal scales (e.g., Bierman and Nichols, 2004; von Blanckenburg, 2005; Codilean et al., 2021; Portenga and Bierman, 2011; Willenbring et al., 2013; Wittmann et al., 2020). Key to the interpretation of measured nuclide concentrations is a quantitative understanding of nuclide production and decay rates throughout the basin from which the sediment is derived.

The ratio of ^{26}Al to ^{10}Be at production is ~6.8 at low and mid latitudes (Balco et al., 2008), but there are subtle influences of latitude and altitude on that ratio (Argento et al., 2015; Halsted et al., 2021; Lifton et al., 2014). Nuclide production decreases exponentially with depth below Earth's surface such that once sediment is buried

more than a meter or two, decay, rather than production systematics, controls the evolution of the $^{26}Al/^{10}Be$ ratio over time (Granger, 2006; Wittmann and von Blanckenburg, 2009).

Landscapes lose mass by both chemical and physical processes. The sum of these processes is referred to as denudation and includes total mass loss integrated over depth. Mass loss rates inferred from cosmogenic nuclide concentrations in sediment have most often referred to as erosion rates (Bierman and Steig, 1996; Granger et al., 1996; Lal, 1991; VanLandingham et al., 2022) and we adopt that convention in this paper. We do this because our data set includes numerous samples from parts of the world where there is deep chemical weathering (the tropics and unglaciated, low-slope temperate regions). In these areas, mass loss through dissolution and groundwater export extends many meters below the penetration depth of the cosmic ray neutrons responsible for most ^{10}Be and ^{26}Al production. Such export of mass in solution is not reflected in the concentration of in situ produced cosmogenic nuclides, which are only sensitive to mass loss in the uppermost few meters of Earth's dynamic surface (e.g., Campbell et al., 2022).

2.2.1 Basin-scale erosion rates from single-nuclide measurements

Basin-scale erosion rates have been estimated around the world by measuring the concentration of a single cosmogenic nuclide, most often in situ ^{10}Be, in samples of amalgamated river sediment (Bierman and Steig, 1996; Brown et al., 1995; Codilean et al., 2022; Granger et al., 1996; Portenga and Bierman, 2011). Sediment grains accumulate ^{10}Be during exhumation and at the surface in source zones, with the nuclide concentration within grains being proportional to the residence time of grains on hillslopes (Heimsath et al., 1997; Jungers et al., 2009). When collecting a sample of fluvial sediment downstream, it is assumed that such a sample represents the average nuclide concentration in grains sourced from all sediment-generating hillslopes within a basin (Bierman and Steig, 1996; Granger et al., 1996; Brown et al., 1995).

Accuracy of basin-scale erosion rate calculations depends upon the validity of several assumptions about sediment generation and transport that cannot be tested with single-nuclide analyses: that sampled grains were steadily exhumed on hillslopes in sediment source zones, are well mixed, and are transported rapidly through fluvial networks such that nuclide production and decay in the transport zone is minimal (Bierman and Steig, 1996; Granger et al., 1996; Brown et al., 1995). This last assumption is most likely to be valid if the volume of sediment stored in the system is small in comparison to the volume of sediment generated and transported through the system on timescales relevant to ^{10}Be production and decay (millennia; Granger et al., 1996).

2.2.2 Sediment routing dynamics from paired ^{10}Be and ^{26}Al

In situ ^{10}Be and ^{26}Al are the most commonly analysed cosmogenic nuclide pair in river sediment, with measurements having started in the late 1990s (Bierman and Caffee, 2001; Clapp et al., 2000, 2001, 2002; Heimsath et al., 1997; Nichols et al., 2002). Their popularity reflects the relative ease of extracting this isotope pair from the same aliquot of quartz, the wide distribution of quartz across landscapes, and because of their contrasting half-lives (1.4 My and 0.7 My, respectively, Chmeleff et al., 2010; Korschinek et al., 2010; Nishiizumi, 2004). When sediment

is buried, the shorter-lived ^{26}Al is preferentially lost as decay exceeds production, and the $^{26}Al/^{10}Be$ ratio in quartz lowers over time (Balco and Rovey, 2008; Granger, 2006).

$^{26}Al/^{10}Be$ ratios lower than those at production have been used as isotopic indicators of sediment storage and subsequent remobilization in catchments across the world, ranging from arid (Bierman et al., 2001; Bierman and Caffee, 2001; Clapp et al., 2002; Kober et al., 2009) to tropical (Campbell et al., 2022; Wittmann et al., 2011) climates and in small (Clapp et al., 2000, 2001) to very large (Ben-Israel et al., 2022; Fülöp et al., 2020; Hidy et al., 2014; Wittmann et al., 2020; Wittmann and von Blanckenburg, 2016) basins. However, in some studies, lowered $^{26}Al/^{10}Be$ ratios were attributed to laboratory errors (Insel et al., 2010; Walcek and Hoke, 2012; Hattanji et al., 2019) or incorporation of meteoric ^{10}Be (Corbett et al., 2022; Moon et al., 2018) and disregarded.

In this study, sediment burial (and resulting preferential loss of shorter-live ^{26}Al by decay) is reflected by the discordance between erosion rates calculated from ^{10}Be (E_{Be}) and ^{26}Al (E_{Al}), the calculation of which normalizes spatial variations in the $^{26}Al/^{10}Be$ surface production ratio and accounts for differential nuclide decay during prolonged surface exposure in very slowly eroding terrains. Thus, calculating erosion rate discordance rather than using nuclide concentration ratios facilitates comparisons between basins across the world and is sensitive only to nuclide decay caused by sediment burial after initial exposure, rather than decay that occurs during prolonged surface or near-surface exposure.

If sediment is transferred from slopes into channels and transported through the channel network without extended burial, then erosion rates calculated from the concentration of each nuclide should be coincident ($E_{Be} = E_{Al}$). Discordance between erosion rates calculated from the two nuclides (unless it is caused by laboratory errors) reflects preferential loss of ^{26}Al when and where decay exceeds production, in which case $E_{Be} < E_{Al}$. This occurs when sediment is stored below the surface (>2m) and for extended periods ($>10^5$ years) after initial surface exposure on hillslopes or in floodplains (Fig. 1).

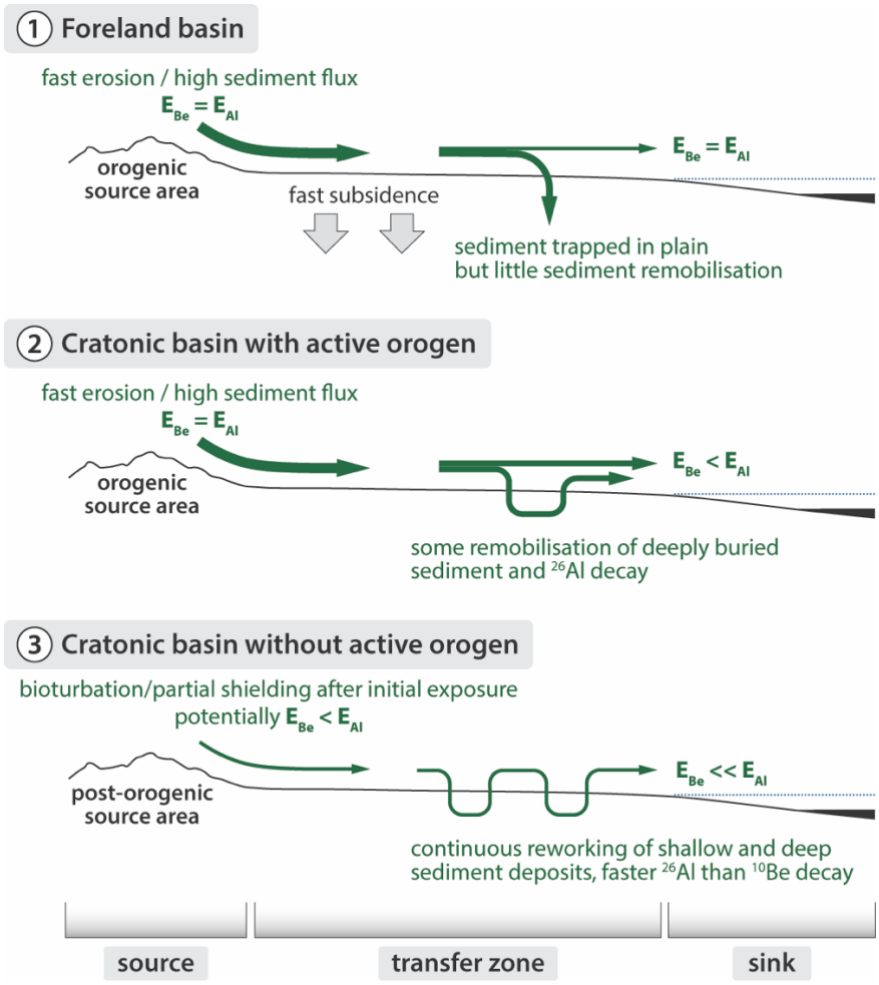

Figure 1: Effects of storage in sediment source and/or transfer zones on ^{10}Be and ^{26}Al-based erosion rates measured in detrital quartz grains. In Panel 1, rapid erosion rates in the source zone and limited remobilization of stored sediment in the transfer zone result in detrital sediment with concurrent erosion rates (E_{Be}/E_{Al} = 1). In Panel 2, rapid erosion rates in the source zone and some remobilization of stored sediment in the transfer zone result in detrital sediment with erosion rate discordance (E_{Be}/E_{Al} < 1), although prolonged sediment storage (>10^5 years) is necessary for erosion rate discordance to be measurable. In Panel 3, slow erosion rates in the source zone and remobilization of stored sediment in the transfer zone result in detrital sediment with substantial erosion rate discordance (E_{Be}/E_{Al} << 1). This figure is based on Figure 6 in Wittmann et al. (2016).

Floodplain sediment storage of <10^5 years has minimal effect on E_{Be}/E_{Al} in sediment grains (Wittmann and von Blanckenburg, 2009), but during prolonged (>10^5 years) storage, especially at depths below which most nuclide production by spallation occurs (> several hundred g cm^{-2}), the E_{Be}/E_{Al} of amalgamated samples can lower sufficiently that the lowering can be detected with confidence in quartz containing moderate to high concentrations of these nuclides (Fig 1). In slowly-eroding terrains (<10 m My^{-1}), long subsurface sediment residence times on hillslopes after initial exposure, due to vertical mixing, can lead to erosion rate discordance in sediment source areas due to preferential ^{26}Al decay before regolith reaches the channel (Fig. 1; Makhubela et al., 2019; Struck et al., 2018). The rate of E_{Be}/E_{Al} lowering is depth-dependent, the ratio decreases more rapidly with increased sediment burial depth as nuclide production rates decrease.

Re-introduction of stored sediment with low E_{Be}/E_{Al} back into the active channel will lower the average E_{Be}/E_{Al} of fluvial sediment in transport (Wittmann et al., 2009; Fig. 1). Geomorphic processes responsible for sediment reworking in transfer zones vary widely depending on basin morphology, tectonics, and climatology. Extensive sediment storage followed by remobilization is documented in meandering, low-lying, tropical river systems (Wittmann et al., 2011), arid river systems that source sediment from sand dunes containing long-buried sediments (Eccleshall, 2019; Vermeesch et al., 2010), hydrologically-variable basins where flood events remobilize vertically-accreted floodplain deposits (Codilean et al., 2021), and formerly glaciated basins where sediments were repeatedly covered by ice (Jautzy et al., 2024). While old, deeply-buried deposits typically have low nuclide concentrations and thus less influence on the average E_{Be}/E_{Al} when mixed with active channel sediment in small amounts, high flow events may re-mobilize substantial volumes of long-buried sediment and have a significant impact on nuclide concentrations (e.g., Codilean et al. 2021; Wittmann et al., 2011) and calculated E_{Be}/E_{Al}.

3 Methods

3.1 Study Design – Approach and Limitations

In this study, we use a compilation of previously-published (n = 649) and new (n = 117) paired ^{10}Be and ^{26}Al concentration measurements in fluvial sediments to assess storage and remobilization during sediment generation and/or transport. We calculate nuclide-specific erosion rates and use the agreement or discordance between these rates to identify burial during transport. We measure the morphometric and climatological properties of basins from which the sampled sediments derive and use a variety of statistical analyses to assess if basin properties are correlated with cosmogenic indications of burial. Then, we consider geomorphic mechanisms to explain observed correlations and discuss the implications of our results for the widely-used basin-averaged ^{10}Be erosion rate method.

Measured ^{26}Al and ^{10}Be alone cannot quantify sediment storage durations or identify specific geomorphic histories for each sample because sediment samples are mixtures of grains with different histories and the inverse solutions are non-unique (Bierman and Steig, 1996; von Blanckenburg, 2005; Brown et al., 1995; Granger et al., 1996; Schaefer et al., 2022). The rate of E_{Be}/E_{Al} lowering in stored sediment is depth-dependent (Wittmann and von Blanckenburg, 2009); thus, the mixing of grains with different storage depth and time histories, and consequently varying histories and duration of nuclide decay and production, precludes accurate estimations of storage duration. Although we identify basin properties that correlate with isotopic indications of burial and storage, the identification of specific processes responsible for storage and subsequent remobilization will differ on a case-by-case basis.

3.2 Data sources

We used two data sources: measurements in reported published studies (n = 649) and ^{26}Al and ^{10}Be concentrations from new ^{26}Al measurements made on samples archived at the University of Vermont (UVM) that had previously published ^{10}Be concentrations (n = 117). For all samples, we normalized originally-reported ^{10}Be concentrations to the 07KNSTD standard (Nishiizumi et al., 2007) and ^{26}Al concentrations to the KNSTD standard

(Nishiizumi, 2004) using conversion factors based on the original AMS standards used for normalization (Table S1; Balco et al., 2008; Nishiizumi et al., 2007).

3.2.1 Sources of previously published paired ^{26}Al and ^{10}Be measurements

We sourced data from the OCTOPUS database (Codilean et al., 2018, 2022; Codilean and Munack, 2024) for previously-published paired ^{26}Al and ^{10}Be measurements from fluvial sediments around the world with robust documentation of processing methods, including the Al and Be standards used during AMS measurements (n = 555). We also compiled samples from studies that had not yet been added to the OCTOPUS database at the time of writing (n = 94; Wang et al., 2017; Adams and Ehlers, 2018; Mason and Romans, 2018; Moon et al., 2018; Hattanji et al., 2019; Hubert-Ferrari et al., 2021; Yang et al., 2021; Zhang et al., 2021; Ben-Israel et al., 2022; Zhang et al., 2022; Jautzy et al., 2024). Previously-published samples were processed at numerous laboratories, including at UVM, and were analyzed at several AMS facilities (sources, raw data, and AMS facilities for previously published samples are reported in Table S1).

3.2.2 Sample processing for new ^{26}Al measurements

Samples with new ^{26}Al measurements come from a wide range of locations but were processed entirely at UVM between 2009 and 2019. These archived samples had previously undergone Be and Al extraction following established methods (Corbett et al., 2016), but only had ^{10}Be concentrations measured (^{10}Be concentration measurements were originally reported in their source publications and are provided in Table S2). The Al-bearing fraction of these archived samples, Al and Be having been separated by column chromatography during the original sample processing for ^{10}Be analysis (Corbett et al., 2016), were stored as Al hydroxide gels.

We re-dissolved the gels into a chloride liquid form using 1 mL of 6 mol/L hydrochloric acid and allowed the gels to sit in acid for several weeks. When completely dissolved, we added 4 mL of water to each sample to create a 1.2 mol/L hydrochloric acid solution for column chromatography and centrifuged the samples to remove any lingering undissolved material. We removed ^{26}Mg, an isobar of ^{26}Al, via column chromatography and then followed the methods outlined in Corbett et al. (2016) to convert samples into an Al oxide powder mixed with Nb for ^{26}Al/^{27}Al measurement via accelerator mass spectrometry (AMS).

^{26}Al/^{27}Al ratios for these re-processed samples were measured using AMS between 2019 and 2021 at the Purdue Rare Isotopes Measurement Laboratory (PRIME), where the addition of a gas-filled magnet to the AMS has significantly reduced ^{26}Al measurement uncertainties (Caffee et al., 2015). Samples were measured against primary standard KNSTD with a ^{26}Al/^{27}Al ratio of 1.818×10^{-12} (Nishiizumi, 2004). We re-processed blanks that were archived with the Al hydroxide gels from their original processing batches (n = 37) and blank-corrected samples by subtracting the estimated ^{26}Al atoms in the batch-specific blank from the total ^{26}Al in the sample (Table S2). Where the original batch blank was missing, likely due to others re-sampling Al gels from the batch prior to 2019, the average ^{26}Al/^{27}Al ratio from all re-processed blanks ($2.37 \pm 1.84 \times 10^{-15}$; 1SD) was used to estimate a blank correction. We propagated AMS ^{26}Al/^{27}Al and blank measurement uncertainties in quadrature to quantify total ^{26}Al

concentration uncertainty. All new ^{26}Al concentration, blank, and uncertainty measurements and calculations can be found in Table S2.

3.3 Calculating ^{10}Be and ^{26}Al-derived erosion rates and erosion rate discordance.

We use the erosion rate calculator formerly known as CRONUS v3 (Balco et al., 2008) with the nuclide-specific LSDn scaling scheme (Lifton et al., 2014) to calculate E_B and E_{Al}. The LSDn scaling scheme depicts spatial variations in the ^{26}Al/^{10}Be surface production ratio (Halsted et al., 2021) and thus calculated E_B and E_{Al} values are normalized to local nuclide-specific production rates to facilitate comparisons across the world. We assumed no shielding and estimate spatially-averaged basin altitude scaling factors using an iterative process that identifies the atmospheric pressure value best matching the spatially averaged Lal/Stone production rate in each basin, a more computationally efficient method than pixel-based approaches for this large compilation and with nearly indistinguishable results (Codilean and Munack, 2024). We propagated 'internal' uncertainties (i.e., analytical uncertainties) of E_{Be} and E_{Al} estimates in quadrature to quantify the 1-sigma (1σ) uncertainty of E_{Be}/E_{Al}.

A E_{Be}/E_{Al} value indistinguishable from 1 (considering 2σ uncertainties) is consistent with a history without burial (but does not necessarily preclude burial and then re-exposure). A E_{Be}/E_{Al} distinguishably lower than 1 is consistent with a history including burial and remobilization of sediment back into the active channel. E_{Be}/E_{Al} values distinguishably higher than 1 are theoretically impossible and likely indicate laboratory processing and/or measurement errors.

3.4 Quantifying basin parameters

For each basin, we calculated ^{10}Be and ^{26}Al-derived erosion rates, mean basin slope, basin area, local relief using a 2 km radius circular moving window, mean annual precipitation, aridity, tectonic activity, dominant lithology, likelihood of stream flow intermittence, glacial cover at the Last Glacial Maximum, and present-day ice cover (data sources and detailed methods are reported in the Supplementary Material). We created basins shapefiles by delineating watersheds upstream of sediment sampling locations (following the procedures used in the OCTOPUS database; Codilean et al., 2022) and used these shapefiles to calculate zonal statistics within each basin. We determined all sampling locations from the source publications or through personal correspondence with the papers' authors. We treated nested basins individually, such that a sample collected in an upstream tributary basin has a separate basin shapefile from the larger, downstream sample with a basin encompassing all upstream tributaries.

3.5 Statistical analyses

We used hypothesis testing methods to determine if physical or climatological characteristics of sample basins correlate significantly with calculated E_{Be}/E_{Al} values. We used correlation analyses between E_{Be}/E_{Al} values and numerical basin parameters (latitude, mean erosion rate, area, mean area, mean slope, mean local relief, annual precipitation, aridity index, intermittent flow probability, percent cover by both Last Glacial Maximum and present ice, and hypsometric integral) and checked for cross-correlation between all basin parameters. We log-transformed

basin areas and basin-averaged ^{10}Be erosion rates prior to correlation analyses to normalize their skewed distribution (Fig. 4) and used the non-parametric Spearman's Correlation Coefficient to evaluate the strength of correlations due to the lingering non-normality of some basin parameter distributions.

We used a forward stepwise regression analysis as in Portenga and Bierman (2011) to create a multi-variate linear model relating E_{Be}/E_{Al} values to basin parameters. This analysis considers all basin parameters but only fits a regression through those that are most statistically important as defined by the change in p-value of the model F-statistic when adding or removing each parameter. We set the probability to enter as $p < 0.05$ and the probability to leave as $p > 0.1$.

We use one-way analysis of variance (ANOVA) and Tukey multiple comparison of means testing (Abdi and Williams, 2010) to assess the magnitude and statistical significance of E_{Be}/E_{Al} value differences between categorical variables (tectonic activity, dominant lithology, region) and to identify threshold values for E_{Be}/E_{Al} differences based on basin areas and hypsometric integrals. We ran the same analyses using the Kruskal-Wallis H test for multiple comparison of medians (MacFarland and Yates, 2016) and obtained nearly identical results to the Tukey MCM testing; we report only the mean results. We used the python libraries *pandas*, *matplotlib*, *cartopy*, *numpy*, *seaborn*, *scipy*, and *statsmodels* to perform all statistical analyses (except for the forward stepwise regression analysis) and create figures, and a Jupyter notebook with coding for all analyses (including the median analyses) is included in the Supplementary Material. We used MATLAB to perform the forward stepwise regression analysis using the '*stepwiselm*' function; a copy of this script can be found in the Supplementary Material.

4 Results

4.1 Dataset statistics

The compilation of basins assembled here (n = 766) has near-global coverage, although there are fewer data from low-latitude regions, especially at high elevations (Figs 2 and 3). Most basins are < 100,000 km^2 (n = 677), while a small number (n = 25) are very large (>1,000,000 km^2; Fig 2). The basins in the compilation encompass a wide range of morphologic and climatic regimes (Fig 4). The distributions of most basin parameters are right-skewed, with most basins having low-to-moderate slope, relief, and precipitation. The basins are underlain by a variety of dominant lithologies and are split almost evenly between those that are tectonically active (n = 411) and those that are post-orogenic (n = 355).

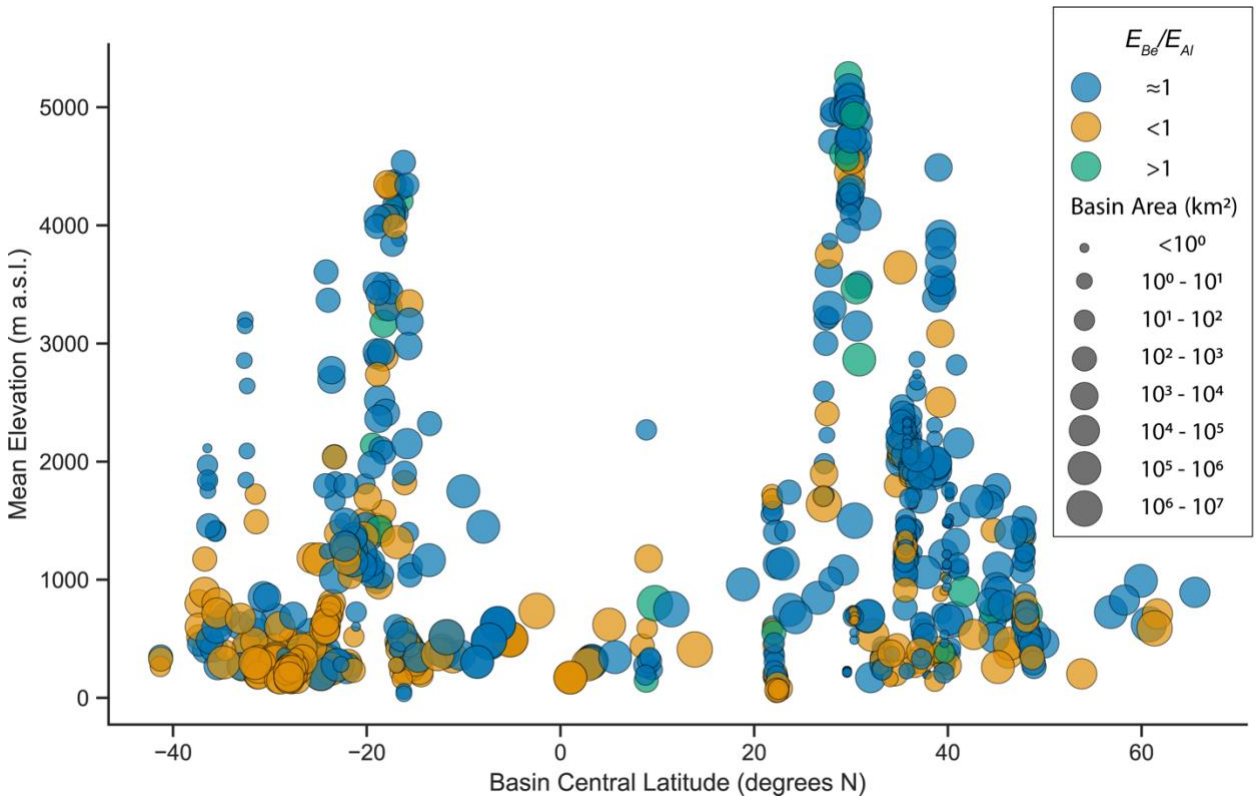

Figure 2. Latitude and elevation distribution of basins in our compilation. Color coding indicates if calculated erosion rate ratios are indistinguishable from 1 (considering 2σ analytical uncertainties), distinguishably lower than 1 or distinguishably higher than 1. The marker size indicates source basin area.

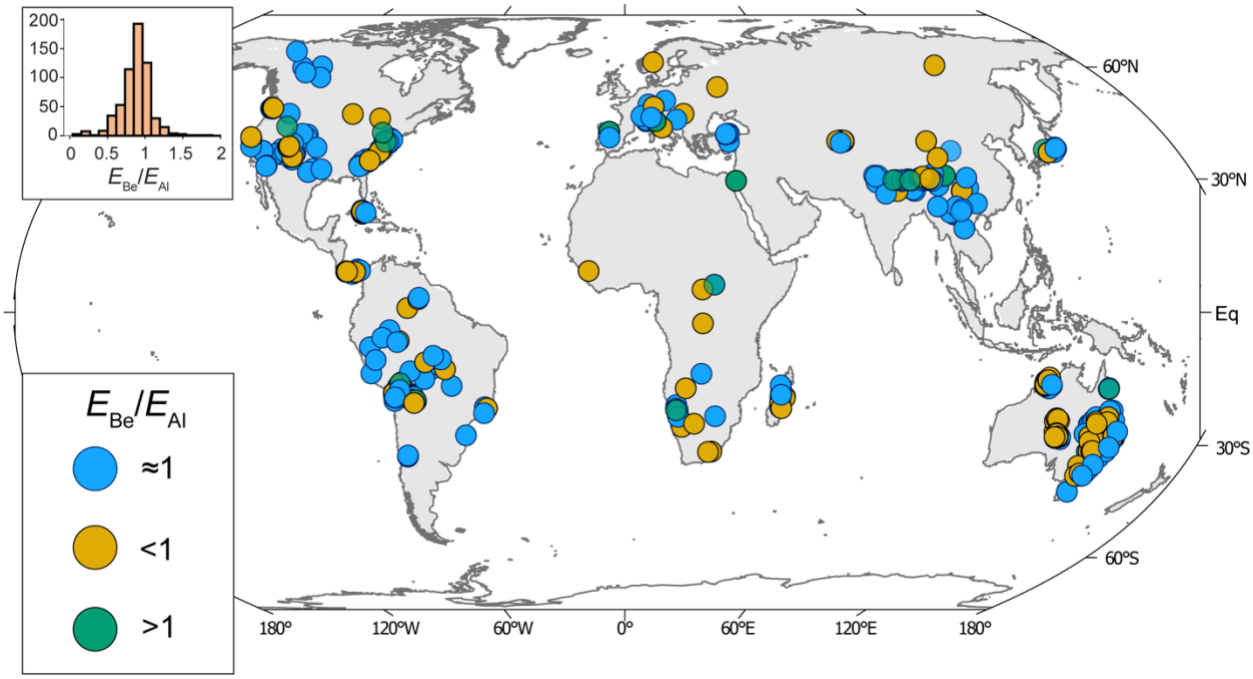

Figure 3. Inset: Distribution of E_{Be}/E_{Al} values. Main: Map of basin centroid locations color-coded by E_{Be}/E_{Al} values.

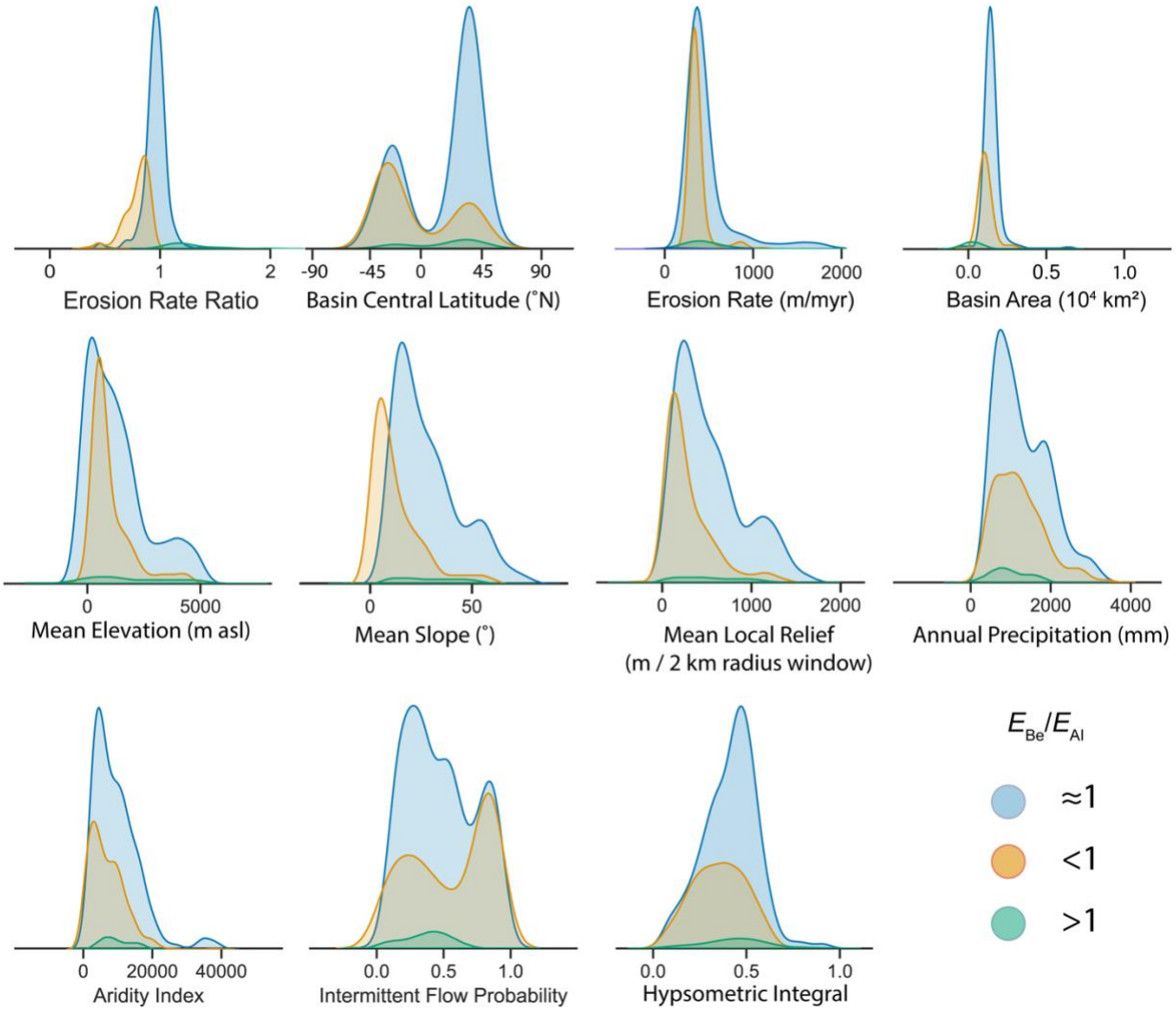

Figure 4. Kernel density distributions of basin parameters with subdivision and color-coding based on E_{Be}/E_{Al} values (see legend). Note that the erosion rate and basin area plots both feature extremely long tails on the high end and thus have x-axis limits imposed. Vertical axes on all plots are relative density values. Sources for all parameters and methods used in their calculations are provided in the Supplementary Materials.

The population of E_{Be}/E_{Al} values (n = 766) approximates a normal distribution with mean = 0.88 and SD = 0.21 (Fig 3 inset). Approximately 31% of the samples in the compilation (n = 238) have E_{Be}/E_{Al} values that are distinguishably lower than 1 when considering 2σ analytical uncertainties, while ~3.5% of samples (n = 27) have E_{Be}/E_{Al} values distinguishably higher than 1.

4.2 Correlation analysis and stepwise regression

Of the basin parameters, all but aridity index exhibit statistically-significant correlations with E_{Be}/E_{Al} values ($p < 0.05$), although none of the correlations with E_{Be}/E_{Al} are particularly strong ($r_s < 0.4$; Figure 5).

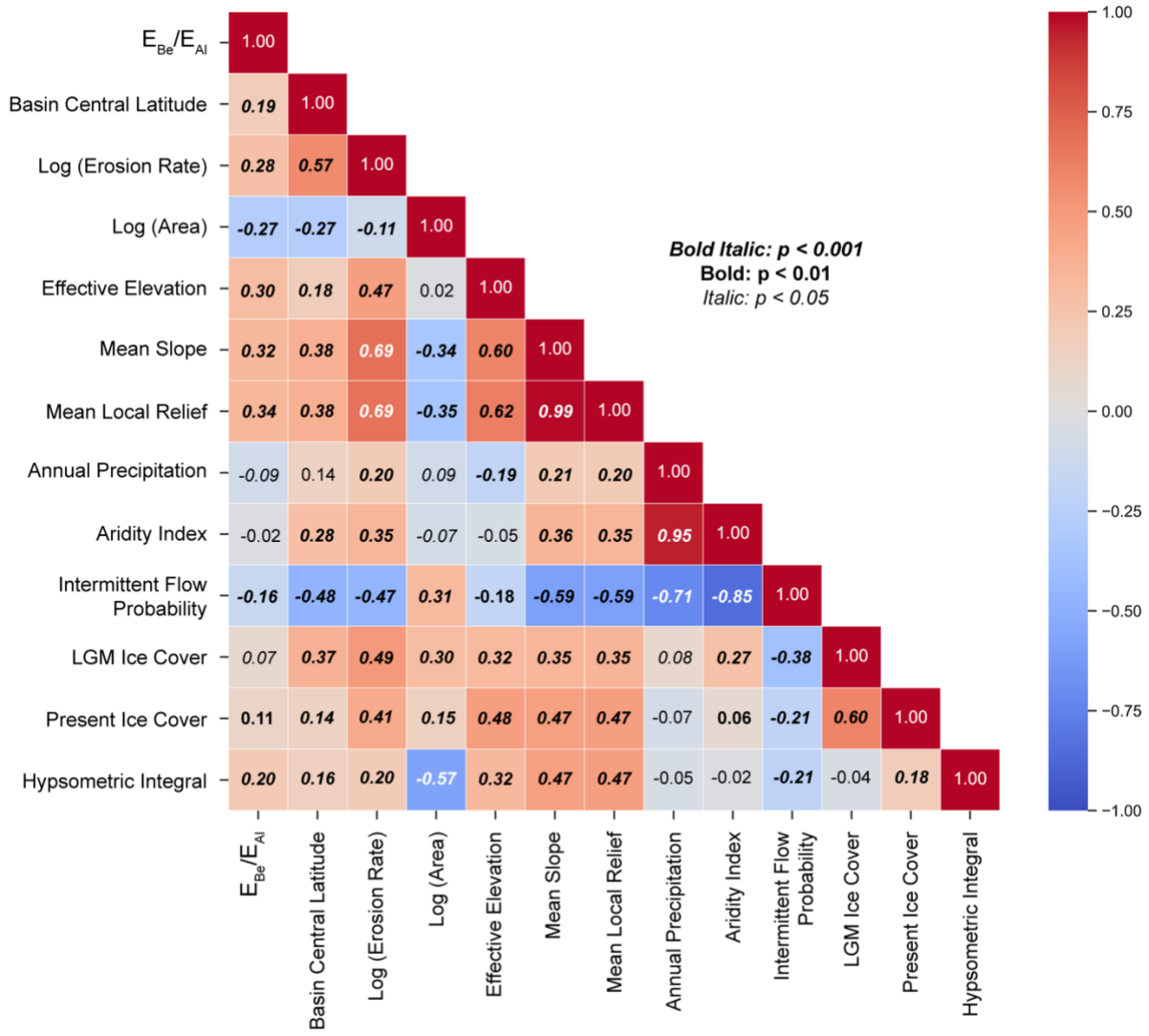

Figure 5. Cross-correlation matrix for basin parameters and E_{Be}/E_{Al} values. Color scale shows Spearman's Correlation Coefficient values and font styling indicates statistical significance (p value) of correlation coefficient.

The best-fitting linear model from the forward stepwise regression analysis (Table 1) predicts a decrease in E_{Be}/E_{Al} values with increasing basin area, decreasing basin-averaged erosion rate, decreasing basin mean elevation, and decreasing hypsometric integral. No other basin parameters improved this multivariate model and thus those parameters were removed during the stepwise regression analysis. This model represents a statistically-significant improvement over a constant model ($p << 0.001$), although a low reduced chi-squared statistic (0.048) suggests that it may overfit the data.

Table 1: Summary of linear model (E_{Be}/E_{Al} ~ β + X + Y) output from forward stepwise regression analysis

	Estimate	SE	tStat	p-value
(Intercept)	0.923	0.040	22.868	1.766e-88
Log(Area)	-0.014	0.002	-5.941	4.308e-09
Log(Erosion Rate)	0.017	0.005	3.597	3.422e-04
Mean Elevation	3.215e-05	7.035e-06	4.571	5.678e-06
Hypsometric Integral	0.163	0.072	2.266	2.376e-02

Number of observations: 765, Error degrees of freedom: 760
Root Mean Squared Error: 0.207, R-squared: 0.111, Adjusted R-Squared: 0.107
F-statistic vs. constant model: 23.8, p-value = 1.49e-18
Reduced Chi-Square: 0.048

4.3 ANOVA testing

ANOVA testing offers more granular insight into the decline of E_{Be}/E_{Al} values with increasing basin area and decreasing hypsometric integral, and among categorical basin parameters suggests that tectonic activity, but not dominant lithology, has a significant correlation with measured E_{Be}/E_{Al} values (Figure 6). Post-hoc tests using group mean and median values produced nearly identical results; mean tests are shown here while the results from median post-hoc tests are included in the supplementary information.

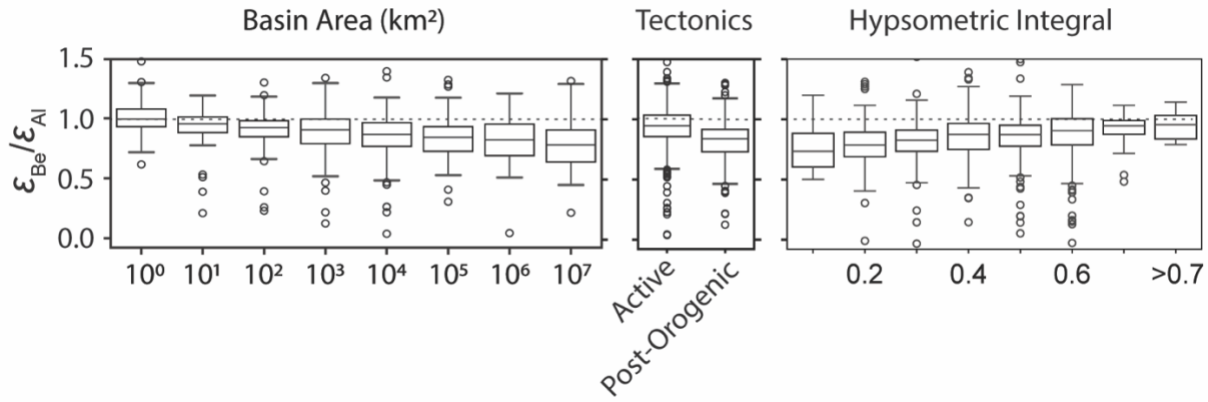

Figure 6. One-way ANOVA results comparing E_{Be}/E_{Al} values between basin area categories (left, basins in each category have areas less than or equal to the label on the x-axis), basin tectonic activity (center), and dominant basin lithology (right). In each plot, boxes show median (center line), 25th and 75th percentile values (box edges) and the maximum and minimum non-outlier values (whiskers). E_{Be}/E_{Al} values plotted as circles are considered outliers (more than 1.5x the interquartile range). The dashed horizontal line in all plots is a reference line for E_{Be}/E_{Al} = 1. Note that n=8 samples have E_{Be}/E_{Al} > 1.5 and are cropped out of this figure.

With basin areas binned on a logarithmic base-10 scale, a decline in E_{Be}/E_{Al} values with increasing basin area is clear (Figure 6; Table 2). Very small basins (≤1 km^2) have a mean E_{Be}/E_{Al} value of approximately 1 (μ = 0.96 ± 0.20, n = 83) while the largest basins (>1,000,000 km^2) have a mean E_{Be}/E_{Al} value of 0.79 ± 0.25 (n = 25). We use

a multi comparison test to assess if E_{Be}/E_{Al} mean values for each basin area category are significantly different than the smallest basin group and find that basins larger than 1,000 km^2 have mean E_{Be}/E_{Al} values less than 1. The percentage of basins with E_{Be}/E_{Al} values that are lower than 1 (considering 2σ uncertainties) increases from 13% in the < 1 km^2 area bin to 40% in the 10^4 km^2 area bin and remains above 35% for all larger basins (Table 2).

Table 2: One-way ANOVA results comparing measured E_{Be}/E_{Al} values between basin area categories. Note that the label for each basin area category shows the upper limit for basin areas in that bin.

Basin Area (km^2)	**n**	**E_{Be}/E_{Al} Mean**	**E_{Be}/E_{Al} S.D.**	**MCMean to 10^0 km^2 basins, p-value***	**% of Basins with E_{Be}/E_{Al} < 1****
10^0	83	0.96	0.20	-	13
10^1	68	0.93	0.28	0.39	15
10^2	119	0.90	0.18	0.13	25
10^3	180	0.88	0.22	0.02	32
10^4	136	0.87	0.21	<0.01	42
10^5	91	0.83	0.22	<0.01	42
10^6	64	0.82	0.17	<0.01	39
10^7	25	0.79	0.25	<0.01	36

**Shows p-value for Tukey multi-comparison of means test performed between basin area category and the smallest basins (<10^0 km^2)*

***Including 2σ uncertainties*

Basin hypsometric integrals also have a statistically significant influence on E_{Be}/E_{Al} based on ANOVA testing (Figure 6; p = 0.007). Mature basins with low hypsometric integrals generally have lower mean E_{Be}/E_{Al} values compared to basins with high hypsometric integrals, but a multi comparison of means test demonstrates that these differences are not statistically significant (Table 3). The percentage of basins with E_{Be}/E_{Al} values that are lower than 1 (considering 2σ uncertainties) increases from 9% in the >0.7 hypsometric integral bin to >30% for basins with hypsometric integrals <0.4 (Table 3).

Table 3: One-way ANOVA results comparing measured E_{Be}/E_{Al} values between hypsometric integral categories. Note that the label for each hypsometric integral category shows the upper limit for the integral in that bin.

Hypsometric Integral	**n**	**E_{Be}/E_{Al} Mean**	**E_{Be}/E_{Al} S.D.**	**MCMean to >0.7 basins, p-value***	**% of Basins with E_{Be}/E_{Al} < 1****
0.1	22	0.81	0.21	0.09	36
0.2	60	0.83	0.24	0.07	48
0.3	115	0.84	0.20	0.08	43
0.4	164	0.89	0.23	0.38	34

0.5	215	0.89	0.22	0.39	26
0.6	147	0.89	0.22	0.35	22
0.7	31	0.95	0.13	0.93	23
>0.7	11	1.04	0.29	-	9

**Shows p-value for Tukey multi-comparison of means test performed between hypsometric integral category and the category >0.7.*

***Including 2σ uncertainties*

We find that basins in tectonically active settings have higher E_{Be}/E_{Al} values ($\mu = 0.93 \pm 0.22$, n = 411) than post-orogenic basins ($\mu = 0.83 \pm 0.20$, n = 355); this difference is statistically significant ($p << 0.01$). Dominant basin lithology has less influence on E_{Be}/E_{Al} values (Table 4). Most lithologies have mean E_{Be}/E_{Al} values that are statistically indistinguishable from each other. The exception is basins composed primarily of unconsolidated sediments, which have, on average, lower E_{Be}/E_{Al} values than other lithologies ($\mu = 0.79 \pm 0.22$, n = 105). The presence of glacial deposits in basins, here categorized as basins with more than 10% coverage by Last Glacial Maximum ice (Ehlers et al., 2011), appears to have little influence on erosion rate discordance when considered at this global scale; basins containing glacial deposits have an average E_{Be}/E_{Al} value ($\mu = 0.90 \pm 0.25$, n = 117) indistinguishable from those without glacial deposits ($\mu = 0.88 \pm 0.21$, n = 649).

Table 4: Mean $E_{Be}/D\backslash E_{Al}$ values and standard deviations for dominant basin lithologies as defined in the GLiM database (Hartmann and Moosdorf, 2012)

Lithology	n	E_{Be}/E_{Al} Mean	E_{Be}/E_{Al} S.D.
Acid Plutonic	134	0.93	0.24
Acid Volcanic	29	0.94	0.16
Basic Volcanic	14	0.92	0.20
Carbonate Sedimentary	28	0.94	0.39
Intermediate Volcanic	9	0.77	0.32
Metamorphic	104	0.90	0.17
Mixed Sedimentary	107	0.93	0.21
Pyroclastic	6	0.86	0.18
Siliciclastic Sedimentary	226	0.86	0.18
Unconsolidated Sediments	105	0.79	0.22

5 Discussion and implications

5.1 Prevalence and potential mechanisms causing complex sediment histories

We find widespread evidence of sediment histories that likely include extended sediment storage on timescales of $10^5 – 10^6$ years as indicated by E_{Be}/E_{Al} values distinguishably lower than 1 (considering 2σ analytical uncertainties) in over 30% of sampled basins around the world (n = 238). This substantial number of low E_{Be}/E_{Al} values rejects the null hypothesis ($p << 0.001$) of minimal nuclide decay due to sediment storage that is assumed in many single-nuclide erosion rate studies.

The occurrence and magnitude of depressed E_{Be}/E_{Al} values is correlated with several basin morphological parameters, suggesting a systematic and thus predictable relationship between basin morphology and sediment history. Although most physical basin parameters exhibited statistically significant correlations with measured E_{Be}/E_{Al} values (Fig. 2), widespread cross-correlations exist between these parameters and suggest several basin characteristics considered together are more likely to predict sediment histories including extended burial. The number of E_{Be}/E_{Al} values distinguishably higher than 1 (n = 27) is within the range expected due to Poisson-distributed measurement uncertainties and is not statistically significant ($p >> 0.05$).

Stepwise linear regression and ANOVA testing suggests that basin area has the single largest influence on E_{Be}/E_{Al} values (Figs 5 and 6, Tables 1 and 2). The scaling of sediment storage duration with basin area is expected (Pizzuto, 2020), with extended burial leading to significant ^{26}Al decay previously documented in very large basins (Wittmann et al., 2011, 2020). Here we find that the average E_{Be}/E_{Al} value is lower than 1, implying >100,000 years of subsurface sediment storage, in basins as small as 1,000 – 10,000 km^2 ($p = 0.02$). The influence of basin area is

apparent in the southern Appalachian mountains of the United States (Reusser et al., 2015; Table 5), where large (>1,000 km^2, n = 5) basins have a lower average D_{Be}/D_{Al} value (0.81 ± 0.05) than small basins (<30 km^2, n = 7, D_{Be}/D_{Al} = 0.91 ± 0.06, p = 0.017), despite other physical basin parameters being similar.

Extended sediment storage in basins as small as 1,000 km^2 is inconsistent with scaling frameworks that relate sediment storage duration to floodplain area in meandering river systems (e.g., Lauer and Parker, 2008). This suggests other mechanisms facilitate extended sediment burial and re-introduction into the active channel. In such moderately sized basins, a variety of processes could explain extended sediment storage, including rivers cutting into sand dunes containing long-buried sediments (Eccleshall, 2019; Vermeesch et al., 2010), hydrologically-variable basins where flood events remobilize vertically-accreted floodplain deposits (Codilean et al., 2021), and excavation of deeply-buried terrace sediments by outburst floods (Zhang et al., 2021). In source generation zones, particularly on slowly-eroding hillslopes, deep vertical mixing can cause repeated burial on slopes, leading to differential nuclide decay before sediments enter river systems (Makhubela et al., 2019).

Other physical basin parameters play secondary and interlinked roles in determining erosion rate discordance (Fig 5, Table 1). Mean basin slope and elevation are positively correlated with each other and with E_{Be}/E_{Al} values, suggesting that alpine basins—which are typically steeper than lowland basins—produce fluvial sediment that has experienced minimal storage and burial. Similarly, basin-averaged erosion rates and intermittent river flow probability exhibit significant correlations with E_{Be}/E_{Al} values and are negatively correlated to each other, suggesting that slowly-eroding basins that regularly experience intermittent river flow are conducive to sediment storage and burial. The influence of basin slope, elevation, and tectonic activity is observed when comparing basins of similar areas in high-alpine Bhutan (Portenga et al., 2015) and low-lying eastern Australia (Codilean et al., 2021); the Bhutan basins have E_{Be}/E_{Al} values near 1 (0.98 ± 0.06, n = 11) while eastern Australian basins have lower average E_{Be}/E_{Al} values (0.83 ± 0.06, n = 7, p < 0.001) indicating extensive sediment storage (Table 5).

Based on cross-correlations between physical basin parameters, we conclude that sediment sourced from large lowland basins— particularly those over 1,000 km^2, with low average erosion rates, low mean slopes, high hypsometric integrals, and in post-orogenic settings— is more likely to exhibit erosion rate discordance indicative of sediment storage and burial in source and/or transfer zones. Smaller alpine basins, particularly steeper basins with higher average erosion rates in tectonically active regions, are more likely to produce sediment with E_{Be}/E_{Al} values that overlap with 1 (within 2 standard deviation analytical uncertainties), suggesting shorter and shallower sediment storage (<10^5 years). We infer that this is because larger, more gently sloping basins in tectonically quiescent regions offer more opportunities for extended sediment storage in floodplains.

Table 5: D_{Be}/D_{Al} regional case studies

Location	**n**	E_{Be}/E_{Al} **mean**	E_{Be}/E_{Al} **S.D.**	**Mean basin elevation (m a.s.l.)**	**Mean basin slope (°)**	**Mean basin area (km^2)**
Southern Appalachians, USA (small basins; Reusser et al., 2015)	7	0.91	0.06	337	5.5	9

*Southern Appalachians, USA (large basins; Reusser et al., 2015)**	5	0.81	0.05	281	7	6262
*Bhutan alpine basins (Portenga et al., 2015)***	11	0.98	0.08	3373	49.4	164
Lockyer sub-basins, Eastern Australia (Codilean et al., 2021)	7	0.83	0.06	430	15.5	130

**One outlier with E_{Be}/E_{Al} = 0.22 was removed. The low ratio of this sample was attributed to laboratory error in the source publication.*

***For this comparison we removed basins larger than 1000 km^2 (n = 3)*

Climatological variables play only a minor role in the occurrence and magnitude of erosion rate discordance. We found very weak correlations between E_{Be}/E_{Al} mean annual precipitation, and aridity (Fig 5; Table 1). However, intermittent flow probability exhibited a significant negative correlation to E_{Be}/E_{Al} values (Fig 5), suggesting that basins with a higher probability of discontinuous flow for at least one day per year are more likely to contain sediment with an extended history of burial. While fluvial systems that experience intermittent flow are most common in arid and semiarid regions (Costigan et al., 2017), they exist around the world and intermittent flow probability is correlated with a variety of hydrologic, geologic, and morphologic variables in addition to climate regime (Messager et al., 2021; Figure 6). Therefore, we cannot confidently attribute an exclusively climatological root for the correlation between intermittent flow probability and isotopic evidence of sediment burial.

Both low and high E_{Be}/E_{Al} values can be caused by laboratory uncertainty (statistical measurement uncertainty) and biases (inaccurate measurements) that influence measured nuclide concentrations. Critical to the accuracy of ^{26}Al and ^{10}Be measurements by AMS is the quantification of total aluminum and beryllium in samples (the stable isotopes, ^{27}Al and ^{9}Be which are many orders of magnitude greater in concentration that the radionuclides ^{26}Al and ^{10}Be). Native beryllium at detectable levels in quartz is rare but occasionally present (e.g., Portenga et al., 2015), and not all laboratories quantify total Be in samples. Unaccounted-for native ^{9}Be will lower measured ^{10}Be/^{9}Be ratios, lower calculated ^{10}Be concentrations, and increase calculated ^{26}Al/^{10}Be ratios.

The presence of meteoric (atmospherically derived) ^{10}Be, if not completely removed by the quartz purification process (Kohl and Nishiizumi, 1992), will increase measured concentration of in situ ^{10}Be as shown by Corbett et al., (2021). In such cases, its presence lowers measured ^{26}Al/^{10}Be ratios (Corbett et al., 2022; Moon et al., 2018). Given sediment storage and thus extended residence and weathering times in large basins, the persistence of weathered mafic minerals is more likely in smaller basin where sediment has less time to weather during transport.

Conversely, stable aluminum (^{27}Al) is ubiquitous in quartz, meaning that full retention and accurate measurement of that isotope, typically via inductively coupled plasma optical emission spectroscopy after quartz dissolution (ICP-OES; e.g., Corbett et al., 2016), is critical to properly quantifying the concentration of ^{26}Al. Low recovery of total Al before ICP-OES and presence of AlF complexes in ICP solutions results in lower than actual ^{26}Al/^{10}Be ratios (Bierman and Caffee, 2002; Corbett et al., 2016). While some scatter in the data is likely the result of such laboratory errors, the observed systematic correlations between morphological basin parameters and E_{Be}/E_{Al} values suggests that most low ratios are due to geologic, rather than laboratory, processes.

5.2 Implications for cosmogenically-derived erosion rates and understanding landscapes

Our analysis shows that nearly a third of all samples for which multi-nuclide measurements exist have discordance between erosion rates derived from ^{10}Be and ^{26}Al beyond 2σ uncertainty. Although some discordant samples may be the result of laboratory errors, most likely represent the complex history of sediment in drainage basins. Because our regression analysis shows that large, low-slope, low-erosion-rate basins are most likely to have sediment with discordant ^{10}Be and ^{26}Al-derived erosion rates, such complexity is best explained by extended sediment storage (>10^5 years) in low gradient floodplains typical of such basins – sufficient time for decay of ^{26}Al to be reliably measurable (e.g., Wittmann et al., 2011; Wittmann and von Blanckenburg, 2016). However, we also find such discordance in basins as small as 1,000 km^2, demonstrating that extended sediment storage followed by re-entry into active channels occurs in a variety of fluvial settings in addition to large meandering, low-land river systems.

The impact of sediment storage on the veracity of cosmogenically-determined erosion rates is difficult to assess for several reasons. First, sediment samples are a mixture of material, meaning that every sample contains many thousands of sand grains, each of which has its own idiosyncratic history. Such mixing means that any attempt at decay correction will be inaccurate as mixing is a linear process and decay correction is not (Bierman and Steig, 1996). Second, sediment both loses nuclides (through radio decay) and gains nuclides (by production at depth, dominated by muons) while in storage. The resulting nuclide concentration is a convolution of time and depth in storage, where depth is unlikely to be constant through time. Because ^{10}Be has a half-life of 1.4 My, it behaves similarly to a stable isotope on timescales typically of concern to geomorphologists, between 10^5 – 10^6 years. Thus, while low E_{Be}/E_{Al} suggests sediment storage on these timescales, it need not imply that ^{10}Be-derived erosion rates are biased significantly by radiodecay.

We consider E_{Be}/E_{Al} in fluvial sediment samples as a window into watershed processes. Specifically, measuring multiple nuclides in sediment samples is useful to detect sediment storage. Additional field and remote sensing measurements, not now typically done alongside sampling for cosmogenic nuclides, have the potential to better elucidate the processes lowering E_{Be}/E_{Al} and the interpretation of measured ratios. For example, field and remote sensing data could be used estimate both the volume and depth of sediment in storage on lowland floodplains (e.g., Dunne et al., 1998) whereas depth profiles along cut banks and in drill cores could provide quantification of nuclide concentrations in material stored in floodplains with depth (Bierman et al., 2005). Measuring cosmogenic nuclides in samples collected down drainage networks can demonstrate if nuclide activities and ^{26}Al/^{10}Be ratios change with basin area and average slope (Clapp et al., 2002; Reusser et al., 2017). Together, these data will elucidate landscape behavior at a variety of scales and bring a deeper understanding of sediment routing and erosion rates throughout large drainage basis.

6 Conclusions

The discordance between basin-averaged erosion rates derived from in situ cosmogenic ^{10}Be and ^{26}Al in detrital fluvial samples provides insights into geomorphic controls on sediment sourcing and routing dynamics and a

valuable check on the assumption of minimal sediment storage that is central to the widely-used, single-nuclide erosion rate method. We calculated the ratio between ^{10}Be and ^{26}Al-derived erosion rates (E_{Be}/E_{Al}) in a global compilation of detrital fluvial samples with measurements from both nuclides (n = 766, of which n = 117 are new) and found that nearly a third of samples (n = 238) exhibit erosion rate discordance as indicated by $E_{Be}/E_{Al} < 1$ (beyond the bounds of 2σ analytical uncertainties). Low E_{Be}/E_{Al} values in detrital sediments are most likely the result of ^{26}Al decay during extended storage (>10^5 years) on hillslopes or in fluvial networks. Source basin area has the greatest influence on sediment E_{Be}/E_{Al} values, with basins >1,000 km^2 more likely to contain sediment with E_{Be}/E_{Al} significantly less than 1. Other physical basin parameters have secondary and interlinked correlations to E_{Be}/E_{Al}, allowing us to separate basins into two broad categories. Large, low-slope, lowland basins in post-orogenic settings are more likely to produce sediment exhibiting erosion rate discordance indicative of extended sediment storage (>10^5 years). Smaller (<1,000 km^2), steep, alpine basins in tectonically active settings are more likely to produce sediment exhibiting erosion rate agreement indicative of minimal sediment storage (<10^5 years). These results provide global-scale insights into sediment routing system dynamics and demonstrate the utility of a multi-nuclide approach for understanding geomorphic processes at the scale of drainage basins.

Code and Data Availability

The supplementary information for this study, including supplementary data tables, text, and a Jupyter Notebook and Matlab script containing code for the statistical analyses and figure production, are available on public Github and Zenodo repositories that can be found with DOI: 10.5281/zenodo.13345369.

Author Contributions

PB and LC conceptualized the study and acquired funding while CH conducted the investigation. PB and LC provided laboratory resources for cosmogenic nuclide chemical processing and LC supervised CH while he performed the chemistry procedures. MC performed the measurement of ^{26}Al measurements and assisted with interpretation of results. CH and AC were responsible for compiling previously published nuclide measurement and performing geospatial analyses, while CH performed the statistical analyses. CH prepared all data visualizations and prepared the original manuscript draft. CH, PB, LC, AC, and MC worked together to review and edit manuscript drafts, and all agreed on the final draft for journal submission.

Competing Interests

The authors declare that they have no conflict of interest.

References

Abdi, H. and Williams, L. J.: Tukey's Honestly Significant Difference (HSD) Test, in: Encyclopedia of Research Design, Sage, Thousand Oaks, CA, 2010.

Allen, P. A.: Time scales of tectonic landscapes and their sediment routing systems, Geological Society, London, Special Publications, 296, 7–28, 2008.

Allen, P. A.: Sediment Routing Systems: The Fate of Sediment from Source to Sink, Cambridge University Press, Cambridge, https://doi.org/10.1017/9781316135754, 2017.

Argento, D. C., Stone, J. O., Reedy, R. C., and O'Brien, K.: Physics-based modeling of cosmogenic nuclides part II - Key aspects of in-situ cosmogenic nuclide production, Quaternary Geochronology, 26, 44–55, https://doi.org/10.1016/j.quageo.2014.09.005, 2015.

Balco, G. and Rovey, C. W.: An isochron method for cosmogenic-nuclide dating of buried soils and sediments, American Journal of Science, 308, 1083–1114, https://doi.org/10.2475/10.2008.02, 2008.

Balco, G., Stone, J. O., Lifton, N. A., and Dunai, T. J.: A complete and easily accessible means of calculating surface exposure ages or erosion rates from 10Be and 26Al measurements, Quaternary Geochronology, 3, 174–195, https://doi.org/10.1016/j.quageo.2007.12.001, 2008.

Ben-Israel, M., Armon, M., Team, A., and Matmon, A.: Sediment residence times in large rivers quantified using a cosmogenic nuclides based transport model and implications for buffering of continental erosion signals, Journal of Geophysical Research: Earth Surface, 127, e2021JF006417, 2022.

Bierman, P. and Caffee, M.: Cosmogenic exposure and erosion history of Australian bedrock landforms, Geological Society of America Bulletin, 114, 787–803, https://doi.org/10.1130/0016-7606(2002)114, 2002.

Bierman, P. and Steig, E. J.: Estimating rates of denudation using cosmogenic isotope abundances in sediment, Earth Surface Processes and Landforms, 21, 125–139, https://doi.org/10.1002/(SICI)1096-9837(199602)21:2<125::AID-ESP511>3.0.CO;2-8, 1996.

Bierman, P., Clapp, E., Nichols, K., Gillespie, A., and Caffee, M. W.: Using cosmogenic nuclide measurements in sediments to understand background rates of erosion and sediment transport, in: Landscape Erosion and Evolution Modeling, Springer, 89–115, 2001.

Bierman, P. R. and Caffee, M.: Slow Rates of Rock Surface Erosion and Sediment Production Across the Namib Desert and Escarpment, Southern Africa, American Journal of Science, 301, 326–358, https://doi.org/10.2475/ajs.301.4-5.326, 2001.

Bierman, P. R. and Nichols, K. K.: Rock to sediment—slope to sea with 10Be—rates of landscape change, Annu. Rev. Earth Planet. Sci., 32, 215–255, 2004.

Bierman, P. R., Reuter, J. M., Pavich, M., Gellis, A. C., Caffee, M. W., and Larsen, J.: Using cosmogenic nuclides to contrast rates of erosion and sediment yield in a semi-arid, arroyo-dominated landscape, Rio Puerco Basin, New Mexico, Earth Surface Processes and Landforms, 30, 935–953, https://doi.org/10.1002/esp.1255, 2005.

von Blanckenburg, F.: The control mechanisms of erosion and weathering at basin scale from cosmogenic nuclides in river sediment, Earth and Planetary Science Letters, 237, 462–479, https://doi.org/10.1016/j.epsl.2005.06.030, 2005.

Blöthe, J. H. and Korup, O.: Millennial lag times in the Himalayan sediment routing system, Earth and Planetary Science Letters, 382, 38–46, 2013.

Brown, E. T., Stallard, R. F., Larsen, M. C., Raisbeck, G. M., and Yiou, F.: Denudation rates determined from the accumulation of in situ-produced 10Be in the Luquillo Experimental Forest, Puerto Rico, Earth and Planetary Science Letters, 129, 193–202, 1995.

Campbell, M. K., Bierman, P. R., Schmidt, A. H., Sibello Hernández, R., García-Moya, A., Corbett, L. B., Hidy, A. J., Cartas Águila, H., Guillén Arruebarrena, A., and Balco, G.: Cosmogenic nuclide and solute flux data from central Cuban rivers emphasize the importance of both physical and chemical mass loss from tropical landscapes, Geochronology, 4, 435–453, 2022.

Carretier, S., Guerit, L., Harries, R., Regard, V., Maffre, P., and Bonnet, S.: The distribution of sediment residence times at the foot of mountains and its implications for proxies recorded in sedimentary basins, Earth and Planetary Science Letters, 546, 116448, https://doi.org/10.1016/j.epsl.2020.116448, 2020.

Cazes, G., Fink, D., Codilean, A. T., Fülöp, R., Fujioka, T., and Wilcken, K. M.: 26Al/10Be ratios reveal the source of river sediments in the Kimberley, NW Australia, Earth Surface Processes and Landforms, 45, 424–439, 2020.

Chmeleff, J., Von Blanckenburg, F., Kossert, K., and Jakob, D.: Determination of the 10Be half-life by multicollector ICP-MS and liquid scintillation counting, Nuclear Instruments and Methods in Physics Research Section B: Beam Interactions with Materials and Atoms, 268, 192–199, https://doi.org/10.1016/j.nimb.2009.09.012, 2010.

Clapp, E. M., Bierman, P. R., Schick, A. P., Lekach, J., Enzel, Y., and Caffee, M.: Sediment yield exceeds sediment production in arid region drainage basins, Geology, 28, 995–998, https://doi.org/10.1130/0091-7613(2000)28, 2000.

Clapp, E. M., Bierman, P. R., Nichols, K. K., Pavich, M., and Caffee, M.: Rates of sediment supply to arroyos from upland erosion determined using in situ produced cosmogenic 10Be and 26Al, Quaternary Research, 55, 235–245, https://doi.org/10.1006/qres.2000.2211, 2001.

Clapp, E. M., Bierman, P. R., and Caffee, M.: Using 10Be and 26Al to determine sediment generation rates and identify sediment source areas in an arid region drainage basin, Geomorphology, 45, 89–104, https://doi.org/10.1016/s0169-555x(01)00191-x, 2002.

Codilean, A. T. and Munack, H.: Short communication: Updated CRN Denudation datasets in OCTOPUS v2.3, Geochronology Discussions, 1–13, https://doi.org/10.5194/gchron-2024-28, 2024.

Codilean, A. T. and Sadler, P. M.: Tectonic Controls on Himalayan Denudation?, AGU Advances, 2, 2021.

Codilean, A. T., Munack, H., Cohen, T. J., Saktura, W. M., Gray, A., and Mudd, S. M.: OCTOPUS: an open cosmogenic isotope and luminescence database, Earth System Science Data, 10, 2123–2139, https://doi.org/10.5194/essd-10-2123-2018, 2018.

Codilean, A. T., Fülöp, R.-H., Munack, H., Wilcken, K. M., Cohen, T. J., Rood, D. H., Fink, D., Bartley, R., Croke, J., and Fifield, L.: Controls on denudation along the East Australian continental margin, Earth-Science Reviews, 214, 103543, 2021.

Codilean, A. T., Munack, H., Saktura, W. M., Cohen, T. J., Jacobs, Z., Ulm, S., Hesse, P. P., Heyman, J., Peters, K. J., Williams, A. N., Saktura, R. B. K., Rui, X., Chishiro-Dennelly, K., and Panta, A.: OCTOPUS database (v.2), Earth Syst. Sci. Data, 14, 3695–3713, https://doi.org/10.5194/essd-14-3695-2022, 2022.

Corbett, L. B., Bierman, P. R., and Rood, D. H.: An approach for optimizing in situ cosmogenic 10Be sample preparation, Quaternary Geochronology, 33, 24–34, https://doi.org/10.1016/j.quageo.2016.02.001, 2016.

Corbett, L. B., Bierman, P. R., Brown, T. A., Caffee, M. W., Fink, D., Freeman, S. P. H. T., Hidy, A. J., Rood, D. H., Wilcken, K. M., and Woodruff, T. E.: Clean quartz matters for cosmogenic nuclide analyses: An exploration of the importance of sample purity using the CRONUS-N reference material, Quaternary Geochronology, 73, 101403, https://doi.org/10.1016/j.quageo.2022.101403, 2022.

Dosseto, A., Buss, H. L., and Chabaux, F.: Age and weathering rate of sediments in small catchments: The role of hillslope erosion, Geochimica et Cosmochimica Acta, 132, 238–258, https://doi.org/10.1016/j.gca.2014.02.010, 2014.

Dunne, T., Mertes, L. A. K., Meade, R. H., Richey, J. E., and Forsberg, B. R.: Exchanges of sediment between the flood plain and channel of the Amazon River in Brazil, GSA Bulletin, 110, 450–467, https://doi.org/10.1130/0016-7606(1998)110<0450:EOSBTF>2.3.CO;2, 1998.

Eccleshall, S. V.: The why, when, and where of anabranching rivers in the arid Lake Eyre Basin, Doctor of Philosophy thesis, University of Wollongong, 2019.

Ehlers, J., Gibbard, P., and Hughes, P.: Quaternary Glaciations - Extent and Chronology, 2–1108 pp., 2011.

Fülöp, R.-H., Codilean, A. T., Wilcken, K. M., Cohen, T. J., Fink, D., Smith, A. M., Yang, B., Levchenko, V. A., Wacker, L., and Marx, S. K.: Million-year lag times in a post-orogenic sediment conveyor, Science Advances, 6, eaaz8845, 2020.

Granger, D. E.: A review of burial dating methods using 26Al and 10Be, in: In Situ-Produced Cosmogenic Nuclides and Quantification of Geological Processes: Geological Society of America Special Paper 415, edited by: Siame, L. L., Bourles, D. L., and Brown, E. T., Geological Society of America, 1–16, https://doi.org/10.1130/2006.2415(01), 2006.

Granger, D. E. and Schaller, M.: Cosmogenic Nuclides and Erosion at the Watershed Scale, Elements, 10, 369–373, https://doi.org/10.2113/gselements.10.5.369, 2014.

Granger, D. E., Kirchner, J. W., and Finkel, R.: Spatially averaged long-term erosion rates measured from in situ-produced cosmogenic nuclides in alluvial sediment, The Journal of Geology, 104, 249–257, https://doi.org/10.1086/629823, 1996.

Halsted, C. T., Bierman, P. R., and Balco, G.: Empirical Evidence for Latitude and Altitude Variation of the In Situ Cosmogenic 26Al/10Be Production Ratio, Geosciences, 11, 402, 2021.

Hartmann, J. and Moosdorf, N.: The new global lithological map database GLiM: A representation of rock properties at the Earth surface, Geochemistry, Geophysics, Geosystems, 13, https://doi.org/10.1029/2012GC004370, 2012.

Heimsath, A. M., Dietrich, W. E., Nishiizumi, K., and Finkel, R. C.: The soil production function and landscape equilibrium, Nature, 388, 358–361, 1997.

Hidy, A. J., Gosse, J. C., Blum, M. D., and Gibling, M. R.: Glacial–interglacial variation in denudation rates from interior Texas, USA, established with cosmogenic nuclides, Earth and Planetary Science Letters, 390, 209–221, 2014.

Jautzy, T., Rixhon, G., Braucher, R., Delunel, R., Valla, P. G., Schmitt, L., and Team, A.: Cosmogenic (un-)steadiness revealed by paired-nuclide catchment-wide denudation rates in the formerly half-glaciated Vosges Mountains (NE France), Earth and Planetary Science Letters, 625, 118490, https://doi.org/10.1016/j.epsl.2023.118490, 2024.

Jerolmack, D. J. and Paola, C.: Shredding of environmental signals by sediment transport, Geophysical Research Letters, 37, 2010.

Jonell, T. N., Owen, L. A., Carter, A., Schwenniger, J.-L., and Clift, P. D.: Quantifying episodic erosion and transient storage on the western margin of the Tibetan Plateau, upper Indus River, Quaternary Research, 89, 281–306, https://doi.org/10.1017/qua.2017.92, 2018.

Jungers, M. C., Bierman, P. R., Matmon, A., Nichols, K., Larsen, J., and Finkel, R.: Tracing hillslope sediment production and transport with in situ and meteoric 10Be, Journal of Geophysical Research: Earth Surface, 114, https://doi.org/10.1029/2008JF001086, 2009.

Kober, F., Ivy-Ochs, S., Zeilinger, G., Schlunegger, F., Kubik, P., Baur, H., and Wieler, R.: Complex multiple cosmogenic nuclide concentration and histories in the arid Rio Lluta catchment, northern Chile, Earth Surface Processes and Landforms, 34, 398–412, 2009.

Kohl, C. P. and Nishiizumi, K.: Chemical isolation of quartz for measurement of in-situ -produced cosmogenic nuclides, Geochimica et Cosmochimica Acta, 56, 3583–3587, https://doi.org/10.1016/0016-7037(92)90401-4, 1992.

Korschinek, G., Bergmaier, A., Faestermann, T., Gerstmann, U. C., Knie, K., Rugel, G., Wallner, A., Dillmann, I., Dollinger, G., Lierse von Gostomski, C., Kossert, K., Maiti, M., Poutivtsev, M., and Remmert, A.: A new value for the half-life of 10Be by Heavy-Ion Elastic Recoil Detection and liquid scintillation counting, Nuclear Instruments and Methods in Physics Research Section B: Beam Interactions with Materials and Atoms, 268, 187–191, https://doi.org/10.1016/j.nimb.2009.09.020, 2010.

Lal, D.: Cosmic ray labeling of erosion surfaces: in situ nuclide production rates and erosion models, Earth and Planetary Science Letters, 104, 424–439, https://doi.org/10.1016/0012-821x(91)90220-c, 1991.

Langbein, W. B. and Leopold, L. B.: Quasi-equilibrium states in channel morphology, American Journal of Science, 262, 782–794, 1964.

Lauer, J. W. and Parker, G.: Modeling framework for sediment deposition, storage, and evacuation in the floodplain of a meandering river: Theory, Water Resources Research, 44, https://doi.org/10.1029/2006WR005528, 2008.

Leopold, L. B. and Wolman, M. G.: River meanders, Geological Society of America Bulletin, 71, 769–793, 1960.

Lifton, N., Sato, T., and Dunai, T. J.: Scaling in situ cosmogenic nuclide production rates using analytical approximations to atmospheric cosmic-ray fluxes, Earth and Planetary Science Letters, 386, 149–160, https://doi.org/10.1016/j.epsl.2013.10.052, 2014.

MacFarland, T. W. and Yates, J. M.: Kruskal–Wallis H-Test for Oneway Analysis of Variance (ANOVA) by Ranks, in: Introduction to Nonparametric Statistics for the Biological Sciences Using R, edited by: MacFarland, T. W. and Yates, J. M., Springer International Publishing, Cham, 177–211, https://doi.org/10.1007/978-3-319-30634-6_6, 2016.

Makhubela, T., Kramers, J., Scherler, D., Wittmann, H., Dirks, P., and Winkler, S.: Effects of long soil surface residence times on apparent cosmogenic nuclide denudation rates and burial ages in the Cradle of Humankind, South Africa, Earth Surface Processes and Landforms, 44, 2968–2981, 2019.

Moon, S., Merritts, D., Snyder, N., Bierman, P., Sanquini, A., Fosdick, J., and Hilley, G.: Erosion of coastal drainages in the Mendocino Triple Junction region (MTJ), northern California, Earth and Planetary Science Letters, 502, 156–165, 2018.

Munack, H., Blöthe, J. H., Fülöp, R. H., Codilean, A. T., Fink, D., and Korup, O.: Recycling of Pleistocene valley fills dominates 135 ka of sediment flux, upper Indus River, Quaternary Science Reviews, 149, 122–134, https://doi.org/10.1016/j.quascirev.2016.07.030, 2016.

Nichols, K. K., Bierman, P. R., Hooke, R. L., Clapp, E. M., and Caffee, M.: Quantifying sediment transport on desert piedmonts using 10Be and 26Al, Geomorphology, 45, 105–125, https://doi.org/10.1016/S0169-555X(01)00192-1, 2002.

Nishiizumi, K.: Preparation of 26Al AMS standards, Nuclear Instruments and Methods in Physics Research Section B: Beam Interactions with Materials and Atoms, 223–224, 388–392, https://doi.org/10.1016/j.nimb.2004.04.075, 2004.

Nishiizumi, K., Imamura, M., Caffee, M. W., Southon, J. R., Finkel, R. C., and McAninch, J.: Absolute calibration of 10Be AMS standards, Nuclear Instruments and Methods in Physics Research Section B: Beam Interactions with Materials and Atoms, 258, 403–413, https://doi.org/10.1016/j.nimb.2007.01.297, 2007.

Otto, J., Schrott, L., Jaboyedoff, M., and Dikau, R.: Quantifying sediment storage in a high alpine valley (Turtmanntal, Switzerland), Earth Surface Processes and Landforms: The Journal of the British Geomorphological Research Group, 34, 1726–1742, 2009.

Pizzuto, J.: Suspended sediment and contaminant routing with alluvial storage: New theory and applications, Geomorphology, 352, 106983, https://doi.org/10.1016/j.geomorph.2019.106983, 2020.

Portenga, E. W. and Bierman, P. R.: Understanding Earth's eroding surface with 10Be, GSA Today, 21, 4–10, https://doi.org/10.1130/g111a.1, 2011.

Portenga, E. W., Bierman, P., Duncan, C., Corbett, L. B., Kehrwald, N. M., and Rood, D. H.: Erosion rates of the Bhutanese Himalaya determined using in situ-produced 10Be, Geomorphology, 233, 112–126, https://doi.org/10.1016/j.geomorph.2014.09.027, 2015.

Repasch, M., Wittmann, H., Scheingross, J. S., Sachse, D., Szupiany, R., Orfeo, O., Fuchs, M., and Hovius, N.: Sediment Transit Time and Floodplain Storage Dynamics in Alluvial Rivers Revealed by Meteoric 10Be, Journal of Geophysical Research: Earth Surface, 125, e2019JF005419, https://doi.org/10.1029/2019JF005419, 2020.

Reusser, L., Bierman, P., and Rood, D.: Quantifying human impacts on rates of erosion and sediment transport at a landscape scale, Geology, 43, 171–174, 2015.

Reusser, L. J., Bierman, P. R., Rizzo, D. M., Portenga, E. W., and Rood, D. H.: Characterizing landscape-scale erosion using 10Be in detrital fluvial sediment: Slope-based sampling strategy detects the effect of widespread dams, Water Resources Research, 53, 4476–4486, https://doi.org/10.1002/2016WR019774, 2017.

Romans, B. W., Castelltort, S., Covault, J. A., Fildani, A., and Walsh, J.: Environmental signal propagation in sedimentary systems across timescales, Earth-Science Reviews, 153, 7–29, 2016.

Schaefer, J. M., Codilean, A. T., Willenbring, J. K., Lu, Z.-T., Keisling, B., Fülöp, R.-H., and Val, P.: Cosmogenic nuclide techniques, Nature Reviews Methods Primers, 2, 18, https://doi.org/10.1038/s43586-022-00096-9, 2022.

Schumm, S.: The Fluvial System, John Wiley & Sons, New York, 338 pp., 1977.

Struck, M., Jansen, J. D., Fujioka, T., Codilean, A. T., Fink, D., Egholm, D. L., Fülöp, R.-H., Wilcken, K. M., and Kotevski, S.: Soil production and transport on postorogenic desert hillslopes quantified with 10Be and 26Al, GSA Bulletin, 130, 1017–1040, 2018.

Tofelde, S., Bernhardt, A., Guerit, L., and Romans, B. W.: Times Associated With Source-to-Sink Propagation of Environmental Signals During Landscape Transience, Front. Earth Sci., 9, https://doi.org/10.3389/feart.2021.628315, 2021.

VanLandingham, L. A., Portenga, E. W., Lefroy, E. C., Schmidt, A. H., Bierman, P. R., and Hidy, A. J.: Comparison of basin-scale in situ and meteoric ^{10}Be erosion and denudation rates in felsic lithologies across an elevation gradient at the George River, northeast Tasmania, Australia, Geochronology, 4, 153–176, https://doi.org/10.5194/gchron-4-153-2022, 2022.

Vermeesch, P., Fenton, C., Kober, F., Wiggs, G., Bristow, C. S., and Xu, S.: Sand residence times of one million years in the Namib Sand Sea from cosmogenic nuclides, Nature Geoscience, 3, 862–865, 2010.

Willenbring, J. K., Codilean, A. T., and McElroy, B.: Earth is (mostly) flat: Apportionment of the flux of continental sediment over millennial time scales, Geology, 41, 343–346, https://doi.org/10.1130/g33918.1, 2013.

Wittmann, H. and von Blanckenburg, F.: Cosmogenic nuclide budgeting of floodplain sediment transfer, Geomorphology, 109, 246–256, 2009.

Wittmann, H. and von Blanckenburg, F.: The geological significance of cosmogenic nuclides in large lowland river basins, Earth-Science Reviews, 159, 118–141, 2016.

Wittmann, H., von Blanckenburg, F., Maurice, L., Guyot, J. L., and Kubik, P. W.: Recycling of Amazon floodplain sediment quantified by cosmogenic 26Al and 10Be, Geology, 39, 467–470, https://doi.org/10.1130/g31829.1, 2011.

Wittmann, H., Malusà, M. G., Resentini, A., Garzanti, E., and Niedermann, S.: The cosmogenic record of mountain erosion transmitted across a foreland basin: Source-to-sink analysis of in situ 10Be, 26Al and 21Ne in sediment of the Po river catchment, Earth and Planetary Science Letters, 452, 258–271, 2016.

Wittmann, H., Oelze, M., Gaillardet, J., Garzanti, E., and von Blanckenburg, F.: A global rate of denudation from cosmogenic nuclides in the Earth's largest rivers, Earth-Science Reviews, 204, 103147, 2020.

Zhang, X., Cui, L., Xu, S., Liu, C., Zhao, Z., Zhang, M., and Liu-Zeng, J.: Assessing non-steady-state erosion processes using paired 10Be–26Al in southeastern Tibet, Earth Surface Processes and Landforms, 46, 1363–1374, 2021.